IEEE Access
Multidisciplinary | Rapid Review | Open Access Journal

Received 3 October 2022, accepted 26 October 2022, date of publication 4 November 2022, date of current version 9 November 2022.

Digital Object Identifier 10.1109/ACCESS.2022.3219453

RESEARCH ARTICLE

Coordination of a Swarm of Unicycle Robots via First-Order Dynamic Couplings

I. RUIZ-RAMOS[1], A. MORALES[1], AND J. PENA RAMIREZ[2]
[1]Robotics and Advanced Manufacturing Program, CINVESTAV, Saltillo, Coahuila CO 25900, Mexico
[2]Center for Scientific Research and Higher Education at Ensenada (CICESE), Ensenada BC 22860, Mexico

Corresponding author: I. Ruiz-Ramos (isaac.ruiz@cinvestav.mx)

This work was supported by the Mexican Council for Science and Technology, CONACYT, under Grant A1-S-26123.

ABSTRACT Coordination of multi-agent systems is an active and ongoing research topic. In particular, there exist several coordination strategies for multi-agent systems, in which the interaction between the agents is via static couplings, i.e. couplings that are constructed using static feedback. In contrast, this paper presents a novel coordination strategy, which introduces the use of dynamic couplings to coordinate a group of unicycle robots following a desired trajectory. The proposed control-scheme is composed by a nonlinear tracking controller and a first-order dynamic coupling. One advantage of this scheme is that, with respect to an energy index, the energy required by the dynamic coupling to perform a cooperative task is lower than the energy required by a traditional scheme based on static coupling. The stability of the closed-loop system is formally demonstrated by using the Lyapunov theory and the obtained theoretical results are illustrated with numerical simulations and validated through experiments. Also, a comparison of the proposed strategy against a coordination scheme reported in the literature, which is based on traditional static coupling, is provided. The results show that the proposed scheme has some practical implications, including reduction of the steady state error and reduced overshoot during the transient.

INDEX TERMS Coordination, dynamic coupling, energy index, synchronization, unicycle robot.

I. INTRODUCTION

There are many examples in nature, in which the living beings work together: a group of ants carrying food to their nest, groups of animals hunting, flocks in flight or a school of fish swimming to evade the attack of a predator [1]. In the above examples, coordinated motion is the key.

Coordination has the following advantages: great efficiency, scalability, robustness and energy reduction [2], [3]. Therefore, engineers and researchers explore new ways to reproduce the advantages of coordination in multi-agent systems (MAS).

Coordination of MAS is an active and ongoing research topic. Multi-agent systems is composed by: intelligent agents and a distributed computation [4]. The agents can communicate with each other and with the environment, whereas the distributed computation aims to solve computing problems [4]. Also, in the distributed computation, the fundamental goal is to reach a parallelism and synchronization of the involved systems by using data linked for the solving problem [4]. Thus, several works have been reported, in which coordination of MAS is studied for different systems such as: manipulator robots [5], [6], aerial robots [7], mobile robots [8], [9], [10], among others.

Furthermore, there exist different techniques to coordinate mobile robots, v.g. distributed optimization [11], distributed estimation and control [2], [12], [13], [14], distributed formation [15], [16], [17], [18], and the use of neural networks [19], [20].

The swarm control is other technique used to coordinate mobile robots. This technique is proposed to use the advantages of coordination for large groups of relatively simple robots [21]. Moreover, this method uses simple rules to make decisions and plans for actual environment or process [22].

In this context, there exist works where swarm control is designed by using sliding-mode control to coordinate omnidirectional mobile robots [22]. In [23], a cooperative control protocol is used to coordinate subgroups of mobile robots

The associate editor coordinating the review of this manuscript and approving it for publication was Zheng Chen.

surrounding the assigned targets. The case of robust coordination of robot swarms under the presence of unknown disturbances has also been addressed, see e.g. [24], where a robust adaptive controller is proposed, in which the coupling gains are dynamically adjusted.

Consensus is other technique used to solve coordination problems. This is a method in which the agents reach a common agreement [25]. There exist a vast literature on consensus of mobile robotics. For example, in [26], a cooperative adaptive consensus protocol is designed by using backstepping and sliding modes, which allows to cope with the unmoddelled dynamics in the robots. In the case of leader follower schemes, there exist some works where the formation control is achieved by using distributed estimators [27] or input saturation [28]. The case of clusters of mobile robots moving in circular trajectories has also been studied [29]. In [30] and [31], a stabilization in predefined time is considered to achieve the consensus of robots.

Furthermore, the consensus problem of mobile robots is also studied taking into account switching topologies [32], [33], [34], [35], communication load [36], and denial-of-services (DoS) attacks [37]. For these cases, recent results show that the effects of the latency can be reduced by synchronizing the communication of the systems [38], [39].

According to [25], it is common to find overlapped approaches to improve results. In [9], [10], and [8], synchronization is developed using a virtual structure scheme where the controller is designed with the Lyapunov redesign method.

The related works to consensus, synchronization, and swarm control have a common characteristic: the systems are coupled. The coupling is defined like a channel by which the agents/systems can communicate to each other [3]. Moreover, this channel can be either static or dynamic [40].

Currently, the schemes based on consensus, synchronization, and swarm control use the static couplings to communicate the mobile robots, see [8], [9], [10], [22], [23], [24], [26], [28], [29], [30], [31], [32], [33], [34], [35], [36], and [37]. The static coupling only weights the differences between the systems and the result is directly applied to the control law, i.e. there is a direct interaction between the systems [41].

On the other hand, the dynamic coupling conveys an indirect interaction between the involved systems, since the coupling signal is dynamically generated [40], [42], [43], [44], [45], [46]. According to [40], the dynamic coupling has some advantages. For example, although the static coupling is easy to implement, in certain cases, it may fail to induce synchronization in some systems or synchronization can be induced in a network only for a narrow range of coupling strength values. Instead, a dynamic coupling can solve these limitations.

In this work, a nonlinear tracking controller with dynamic coupling for inducing cooperative behaviour in a network of nonholonomic mobile robots, is presented. The main contributions of this work are described as follows:

- A novel coordination strategy for mobile robots is proposed, in which the interaction between the agents takes place via a first order dynamic coupling. This dynamic interaction makes the proposed scheme different form the well-known and widely applied scheme based on static feedback, see [8], [9], [10], [22], [23], [24], [26], [28], [29], [30], [31], [32], [33], [34], [35], [36], and [37].
- A global stability analysis for the closed-loop system by using the Lyapunov theory is conducted. In addition, it is analytically demonstrated that the close-loop is stable for any strongly connected graph and N differential-mobile robots.
- It is provided numerical and experimental evidence, that shows some practical advantages that the proposed scheme has over other one reported in the literature, which is based on static coupling. These advantages include: smaller steady state error, reduced overshoot during the transient, and with respect to an energy index, the energy required by the dynamic coupling to perform a cooperative task is lower than the energy required by a traditional coordination scheme with static coupling.

The outline of this work is as follows: Section 2 shows the preliminaries. The proposed controller and the corresponding stability analysis are presented in Section 3. Section 4 shows the performance of the proposed controller. Section 5 exposes the experimental results and after that, Section 6 provides a comparison of the proposed dynamic coordination scheme to a scheme based on static couplings. Finally, some conclusions are given in Section 7.

II. PRELIMINARIES

Consider a network of N unicycle mobile robots within a formation via a virtual-structure scheme, see Fig. 1. The kinematic model for each robot is given by

$$\dot{\mathbf{q}}_i = \begin{bmatrix} \cos\theta_i & 0 \\ \sin\theta_i & 0 \\ 0 & 1 \end{bmatrix} \begin{bmatrix} v_i \\ \omega_i \end{bmatrix}, \ i = 1, \ldots, N, \tag{1}$$

where $\mathbf{q}_i(t) = [\mathbf{p}_i(t), \theta_i(t)]^T$ is the robot pose respect to the global reference frame (GRF), $\mathbf{p}_i = [x_i(t), y_i(t)]^T$ is the position vector, and $\theta_i(t)$ is the orientation. The control inputs v_i and ω_i are the linear and angular velocities of the robot, respectively. Moreover, each unicycle robot has the following well-known nonholonomic constraint

$$\dot{y}_i \cos\theta_i - \dot{x}_i \sin\theta_i = 0, \tag{2}$$

where $\dot{x}_i$ and $\dot{y}_i$ are the linear velocities on the x and y axis, respectively. Furthermore, the orientation can be obtained from (2), which yields

$$\theta_i = \arctan \frac{\dot{y}_i}{\dot{x}_i}. \tag{3}$$

The formation in the virtual-structure scheme has a virtual-center (VC), which follows a desired pose with respect to the

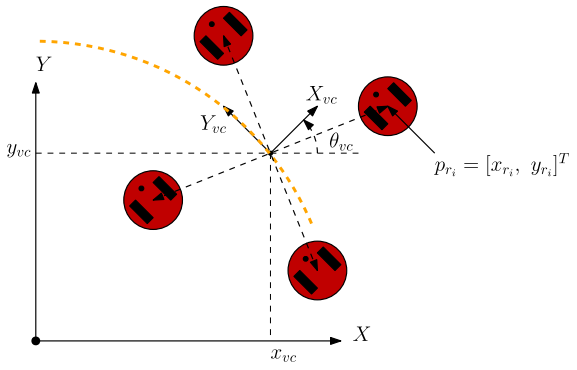

FIGURE 1. Virtual structure scheme. The robots are represented by the red circles and they are located in positions respect to the virtual center, which is following a desired pose (orange dashed line).

GRF, described by $\mathbf{q}_{vc} = [p_{vc}^T, \theta_{vc}]^T$ where $p_{vc} = [x_{vc}, y_{vc}]^T$ is the position of the VC and θ_{vc} is its orientation, see Fig. 1.

Moreover, each robot has a position $\hat{\mathbf{p}}_i = [\hat{x}_i, \hat{y}_i]^T$ with respect to the VC. The reference pose $\mathbf{q}_{r_i}(t) = [\mathbf{p}_{r_i}(t), \theta_{r_i}(t)]^T$ $(i = 1, \ldots, N)$ for each robot with respect to the GRF, is given by the homogeneous transformation

$$\mathbf{q}_{r_i}(t) = \begin{bmatrix} \mathbf{p}_{r_i}(t) \\ \theta_{r_i} \end{bmatrix} = \begin{bmatrix} \mathbf{p}_{vc}(t) + \mathbf{R}(\theta_{vc})\hat{\mathbf{p}}_i \\ \arctan\left(\frac{\dot{y}_{r_i}(t)}{\dot{x}_{r_i}(t)}\right) \end{bmatrix}, \tag{4}$$

where $\mathbf{p}_{r_i}(t) = [x_{r_i}, y_{r_i}]^T$ is the reference position for each robot and $\mathbf{R}(\theta_{vc}) \in R^{2\times 2}$ is a rotational matrix which is given by

$$\mathbf{R}(\theta_{vc}) = \begin{bmatrix} \cos\theta_{vc} & -\sin\theta_{vc} \\ \sin\theta_{vc} & \cos\theta_{vc} \end{bmatrix}. \tag{5}$$

The reference orientation θ_{r_i} of each robot, see (4), depends on the reference velocities on each axis. These velocities can be obtained by

$$\dot{\mathbf{p}}_{r_i} = \dot{\mathbf{p}}_{vc} + \dot{\theta}_{vc}\mathbf{S}\mathbf{R}(\theta_{vc})\hat{\mathbf{p}}_i,\ i = 1, \ldots, N, \tag{6}$$

where $\mathbf{S}$ is a 2×2 skew-symmetric matrix given by

$$\mathbf{S} = \begin{bmatrix} 0 & -1 \\ 1 & 0 \end{bmatrix}. \tag{7}$$

It is considered constant positions $\hat{\mathbf{p}}_i$ $(i = 1, \ldots, N)$, for that reason it is not added the time-derivative of $\hat{\mathbf{p}}_i$.

The robots and their references have the same constraints, compare (3) and (4). Therefore, each reference pose $(\mathbf{q}_{r_i})$ has the same kinematic model for the unicycle robot, i.e.

$$\dot{\mathbf{q}}_{r_i} = \begin{bmatrix} \cos\theta_{r_i} & 0 \\ \sin\theta_{r_i} & 0 \\ 0 & 1 \end{bmatrix} \begin{bmatrix} v_{r_i} \\ \omega_{r_i} \end{bmatrix},\ i = 1, \ldots, N. \tag{8}$$

where v_{r_i} and ω_{r_i} are the reference velocities given by

$$v_{r_i} = \|\dot{\mathbf{p}}_{r_i}\|_2,\ \omega_{r_i} = -\frac{\langle \dot{\mathbf{p}}_{r_i}, \mathbf{S}\ddot{\mathbf{p}}_{r_i} \rangle}{v_{r_i}^2},\ i = 1, \ldots, N, \tag{9}$$

with $\dot{\mathbf{p}}_{r_i}$ and $\mathbf{S}$ defined in (6) and (7), respectively, and

$$\ddot{\mathbf{p}}_{r_i} = \ddot{\mathbf{p}}_{vc} + \left(\ddot{\theta}_{vc}\mathbf{S} - \dot{\theta}_{vc}^2\mathbf{I}^{2\times 2}\right)\mathbf{R}(\theta_{vc})\hat{\mathbf{p}}_i,\ i = 1, \ldots, N, \tag{10}$$

with $\mathbf{I}^{2\times 2}$ as the identity matrix.

A. TRACKING ERRORS

The tracking errors are defined by

$$\begin{bmatrix} \mathbf{e}_i \\ e_{\theta_i} \end{bmatrix} = \begin{bmatrix} \mathbf{R}^T(\theta_i) & \mathbf{0}^{2\times 1} \\ \mathbf{0}^{1\times 2} & 1 \end{bmatrix} \left(\mathbf{q}_{r_i} - \mathbf{q}_i\right),\ i = 1, \ldots, N, \tag{11}$$

where $\mathbf{e}_i = [e_{x_i}, e_{y_i}]^T$ is the error in position, e_{θ_i} is the error in orientation, and $\mathbf{R}(\theta_i)$ is the rotational matrix respect to the GRF for the i-th robot which is given by

$$\mathbf{R}(\theta_i) = \begin{bmatrix} \cos\theta_i & -\sin\theta_i \\ \sin\theta_i & \cos\theta_i \end{bmatrix},\ i = 1, \ldots, N. \tag{12}$$

Then, the errors on the GRF are transformed to the robot reference frame (RRF), in (11), for easing the computing of the control law, see [8].

The dynamic of the tracking errors can be obtained by the time-derivative of (11) where $\dot{\mathbf{q}}_i$ and $\dot{\mathbf{q}}_{r_i}$ are given by (1) and (8), respectively. Therefore,

$$\begin{bmatrix} \dot{\mathbf{e}}_i \\ \dot{e}_{\theta_i} \end{bmatrix} = \begin{bmatrix} \omega_i\mathbf{S}\mathbf{e}_i + \mathbf{G}_i \\ \omega_{r_i} - \omega_i \end{bmatrix},\ i = 1, \ldots, N, \tag{13}$$

where

$$\mathbf{G}_i = \begin{bmatrix} v_{r_i}\cos e_{\theta_i} - v_i \\ v_{r_i}\sin e_{\theta_i} \end{bmatrix}. \tag{14}$$

B. SYNCHRONIZATION ERRORS

The connections in the network can be defined in terms of the Laplacian matrix

$$\mathbf{L} = \begin{bmatrix} \sum_{i=2}^{N} l_{1i} & -l_{12} & \cdots & -l_{1N} \\ -l_{21} & \sum_{i=1, i\neq 2}^{N} l_{2i} & \cdots & -l_{2N} \\ \vdots & \vdots & \ddots & \vdots \\ -l_{N1} & -l_{N2} & \cdots & \sum_{i=1}^{N-1} l_{Ni} \end{bmatrix}, \tag{15}$$

where $l_{ij} \geq 0\ \forall\ i \neq j,\ (i, j) = 1, \ldots, N$.

Furthermore, let $\mathcal{S} = \{1, \ldots, N\}$ be the set of all the robots in a network and $\mathcal{S}_2$ the set for all pairs of robots. Considering $\mathcal{S}_2$, there is a set $\mathcal{N} = \{(i, j)\}$, for all of the connections, in which $l_{ij} > 0$ or $l_{ji} > 0$. This set is given by

$$\mathcal{N} = \{(i, j) \in \mathcal{S}_2 | l_{ij} > 0 \cup l_{ji} > 0\}. \tag{16}$$

The synchronization errors are defined pairwise as follows

$$\begin{bmatrix} \boldsymbol{\epsilon}_{xy_{ij}} \\ \epsilon_{\theta_{ij}} \end{bmatrix} = \begin{bmatrix} \mathbf{e}_i \\ e_{\theta_i} \end{bmatrix} - \begin{bmatrix} \mathbf{e}_j \\ e_{\theta_j} \end{bmatrix},\ (i, j) \in \mathcal{N}, \tag{17}$$

where $\boldsymbol{\epsilon}_{xy_{ij}} = [\epsilon_{x_{ij}},\ \epsilon_{y_{ij}}]^T$ are the synchronization errors for the x and y axis, and the $\epsilon_{\theta_{ij}}$ are the synchronization errors in orientation.

Also, note that the synchronization errors (17) satisfy

$$\begin{bmatrix} \boldsymbol{\epsilon}_{xy_{ji}} \\ \epsilon_{\theta_{ji}} \end{bmatrix} = -\begin{bmatrix} \boldsymbol{\epsilon}_{xy_{ij}} \\ \epsilon_{\theta_{ij}} \end{bmatrix},\ (i, j) \in \mathcal{N}. \tag{18}$$

Finally, the dynamic behaviour of (17) is given by

$$\begin{bmatrix} \dot{\boldsymbol{\epsilon}}_{xy_{ij}} \\ \dot{\epsilon}_{\theta_{ij}} \end{bmatrix} = \begin{bmatrix} \omega_i\mathbf{S}\mathbf{e}_i - \omega_j\mathbf{S}\mathbf{e}_j + \mathbf{G}_i - \mathbf{G}_j \\ \omega_{r_i} - \omega_{r_j} - \omega_i + \omega_j \end{bmatrix}, \tag{19}$$

with $(i, j) \in \mathcal{N}$.

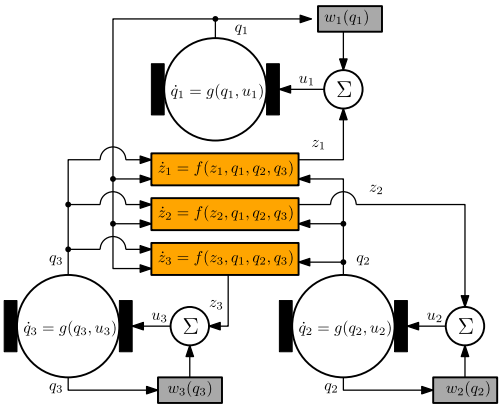

FIGURE 2. Proposed control-scheme. It can be seen that each robot has a tracking controller (gray rectangles) and a dynamic coupling (orange rectangles). The tracking controller will follow the reference pose (4) **meanwhile the dynamic coupling will synchronize the robots to keep the formation.**

C. PROBLEM STATEMENT

Given a network of unicycle robots defined in (1), the problem to be addressed in this work is how to achieve tracking of a desired trajectory while maintaining a desired formation in the robots.

To solve this problem, it is proposed a coordination scheme, in which each robot is endowed with a first order dynamic controller (dynamic coupling) such that the interactions between the robots become indirect. This is schematically depicted in Fig. 2, where the dynamic interconnections for inducing synchronization are indicated by the orange rectangles, whereas the tracking controllers are indicated by the gray boxes.

Furthermore, besides proving the global stability of the closed-loop system and providing an experimental validation, it is desired to determine the potential advantages of the proposed dynamic coordination scheme by means of a comparison to a scheme reported in the literature, which uses classical static feedback.

III. PROPOSED CONTROL

The proposed controller is given by

$$v_i = v_{r_i}\cos e_{\theta_i} + k_x e_{x_i} + C_i z_{x_i}, \tag{20}$$

$$\omega_i = \omega_{r_i} + k_\theta e_{\theta_i} + \frac{Kk_y}{\alpha_i} v_{r_i} e_{y_i} \operatorname{sinc} e_{\theta_i}, \tag{21}$$

for $i = 1, \ldots, N$, where v_{r_i} and ω_{r_i} are the linear and angular velocities defined in (13), $k_x > 0$, $k_y > 0$ are weighting gains for the errors on x and y axis, respectively, whereas $k_\theta > 0$ weights the orientation errors. The function $\operatorname{sinc}(\cdot)$ is defined as follows: $\operatorname{sinc} e_{\theta_i} = \left(\sin e_{\theta_i}\right)/e_{\theta_i}$, with α_i given by

$$\alpha_i = \sqrt{K^2 + e_{x_i}^2 + e_{y_i}^2}, \tag{22}$$

where K is a constant introduced to avoid indefiniteness of (21) when $e_{x_i} = e_{y_i} = 0$. Moreover, C_i is defined by

$$C_i = \begin{cases} 1, & l_{ii} \neq 0 \\ 0, & l_{ii} = 0, \end{cases} \tag{23}$$

with l_{ii} being an element of the main diagonal of the Laplacian matrix (15).

Finally, the coupling signal z_{x_i} in (20) is dynamically generated by the following first-order system

$$\dot{z}_{x_i} = -\alpha z_{x_i} + \mu \sum_{(i,j)\in\mathcal{N}} \sigma_{ij}\epsilon_{x_{ij}},\ i = 1, \ldots, N, \tag{24}$$

where $\alpha > 0$ is a design parameter, $\mu > 0$ is the coupling strength, $\epsilon_{x_{ij}}$ $(i, j) \in \mathcal{N}$ are the synchronization errors on the x-axis in (17), and

$$\sigma_{ij} = \begin{cases} l_{ij}, & i < j \\ -l_{ji}, & i > j, \end{cases} \qquad \forall\,(i,j) \in \mathcal{N} \tag{25}$$

with l_{ij} and l_{ji} being elements of the Laplacian matrix (15).

Remark 1: From (24) *it follows that, when the synchronization errors $\epsilon_{x_{ij}}$ vanish then all the dynamic coupling signals z_{x_i} will decay asymptotically.*

By replacing (20)-(21) in (13) and (19), and considering (24) also as an 'error' due to Remark 1, we obtain the following extended error dynamics, which are composed by tracking errors, synchronization errors and the states of the dynamic interconnections

$$\dot{\mathbf{e}}_x = \Omega_r \mathbf{e}_y + k_\theta \mathbf{e}_{y\theta} + \Gamma_{\operatorname{sinc}\theta}\Gamma_\alpha \mathbf{e}_{y^2} - k_x \mathbf{e}_x - \mathbf{C}\boldsymbol{\zeta}_x, \tag{26}$$

$$\dot{\mathbf{e}}_y = \boldsymbol{\gamma}_{\sin\theta} - \Omega_r \mathbf{e}_x - k_\theta \mathbf{e}_{x\theta} - \Gamma_{\operatorname{sinc}\theta}\Gamma_\alpha \mathbf{e}_{xy}, \tag{27}$$

$$\dot{\mathbf{e}}_\theta = -k_\theta \mathbf{e}_\theta - \Gamma_{\operatorname{sinc}\theta}\Gamma_\alpha \mathbf{e}_y, \tag{28}$$

$$\dot{\boldsymbol{\zeta}}_x = -\alpha\boldsymbol{\zeta}_x + \mu\hat{\mathbf{L}}\boldsymbol{\epsilon}_x, \tag{29}$$

$$\dot{\boldsymbol{\epsilon}}_x = \mathbf{D}\left(\Omega_r \mathbf{e}_y + k_\theta \mathbf{e}_{y\theta} + \Gamma_{\operatorname{sinc}\theta}\Gamma_\alpha \mathbf{e}_{y^2}\right) - k_x\boldsymbol{\epsilon}_x - \mathbf{D}\mathbf{C}_x\boldsymbol{\zeta}_x, \tag{30}$$

$$\dot{\boldsymbol{\epsilon}}_y = \mathbf{D}\left(\boldsymbol{\gamma}_{\sin\theta} - \Omega_r \mathbf{e}_x - k_\theta \mathbf{e}_{x\theta} - \Gamma_{\operatorname{sinc}\theta}\Gamma_\alpha \mathbf{e}_{xy}\right), \tag{31}$$

$$\dot{\boldsymbol{\epsilon}}_\theta = -k_\theta\boldsymbol{\epsilon}_\theta - \mathbf{D}\Gamma_{\operatorname{sinc}\theta}\Gamma_\alpha \mathbf{e}_y, \tag{32}$$

where: $\mathbf{e}_x = [e_{x_1}, \ldots, e_{x_N}]^T$, $\mathbf{e}_y = [e_{y_1}, \ldots, e_{y_N}]^T$, $\mathbf{e}_\theta = [e_{\theta_1}, \ldots, e_{\theta_N}]^T$, $\boldsymbol{\zeta}_x = [z_{x_1}, \ldots, z_{x_N}]^T$, $\mathbf{e}_{y^2} = [e_{y_1}^2, \ldots, e_{y_N}^2]^T$, $\mathbf{e}_{xy} = [e_{x_1}e_{y_1}, \ldots, e_{x_N}e_{y_N}]^T$, $\mathbf{e}_{x\theta} = [e_{x_1}e_{\theta_1}, \ldots, e_{x_N}e_{\theta_N}]^T$, $\mathbf{e}_{y\theta} = [e_{y_1}e_{\theta_1}, \ldots, e_{y_N}e_{\theta_N}]^T$, $\mathbf{C} = \operatorname{diag}(C_1, \ldots, C_N)$, $\Omega_r = \operatorname{diag}(\omega_{r_1}, \ldots, \omega_{r_N})$ whit ω_{r_i} defined in (9), $\boldsymbol{\gamma}_{\sin\theta} = [v_{r_1}\sin e_{\theta_1}, \ldots, v_{r_N}\sin e_{\theta_N}]^T$, $\Gamma_{\operatorname{sinc}\theta} = \operatorname{diag}\left(v_1^r \operatorname{sinc} e_{\theta_1}, \ldots, v_N^r \operatorname{sinc} e_{\theta_N}\right)$, $\Gamma_\alpha = \operatorname{diag}\left(Kk_y/\alpha_1, \ldots, Kk_y/\alpha_N\right)$.

Furthermore, the synchronization errors ϵ_x, ϵ_y, and ϵ_θ, see (30)-(32), are given by

$$\boldsymbol{\epsilon}_x = \mathbf{D}\mathbf{e}_x,\ \boldsymbol{\epsilon}_y = \mathbf{D}\mathbf{e}_y,\ \boldsymbol{\epsilon}_\theta = \mathbf{D}\mathbf{e}_\theta, \tag{33}$$

where matrix $\mathbf{D} \in \mathbb{R}^{\operatorname{card}(\mathcal{N})\times N}$ is a transformation matrix from tracking errors to synchronization errors according to (17).

On the other hand, $\hat{\mathbf{L}} \in \mathbb{R}^{N\times\operatorname{card}(\mathcal{N})}$ is formed by the weights of σ_{ij}, see (25), and in this work, it is referred to as extended Laplacian matrix, and satisfies the following relationship:

$$\mathbf{L} = \hat{\mathbf{L}}\mathbf{D}. \tag{34}$$

A. STABILITY ANALYSIS

The stability properties of the extended error dynamics (26)-(32) are determined using standard Lyapunov analysis and are summarized in the following result.

Theorem 1: Consider a network of N unicycle robots as given in (1) *with control inputs* (20)-(21) *and dynamic interconnections* (24)*. Then, if the controller gains* k_x, k_y, k_θ, K *and* C_i *and the coupling parameters* α, μ *are positive, then the origin of the extended error dynamics* (26)-(32) *is globally asymptotically stable.*

Proof: Consider the Lyapunov function

$$V(\boldsymbol{\vartheta}) = V_{sys}(\boldsymbol{\vartheta}) + V_{cou}(\boldsymbol{\vartheta}) + V_{syn}(\boldsymbol{\vartheta}), \tag{35}$$

where $\boldsymbol{\vartheta} = [\mathbf{e}_x^T,\ \mathbf{e}_y^T,\ \mathbf{e}_\theta^T,\ \boldsymbol{\zeta}_x^T,\ \boldsymbol{\epsilon}_x^T,\ \boldsymbol{\epsilon}_y^T,\ \boldsymbol{\epsilon}_\theta^T]^T$ and

$$V_{sys}(\boldsymbol{\vartheta}) = \frac{1}{2}\left(\mathbf{e}_x^T\mathbf{e}_x + \mathbf{e}_y^T\mathbf{e}_y + \mathbf{e}_\theta^T\mathbf{e}_\theta\right), \tag{36}$$

$$V_{cou}(\boldsymbol{\vartheta}) = \frac{1}{2}\boldsymbol{\zeta}_x^T\boldsymbol{\zeta}_x, \tag{37}$$

$$V_{syn}(\boldsymbol{\vartheta}) = \frac{1}{2}\left(\boldsymbol{\epsilon}_x^T\boldsymbol{\epsilon}_x + \boldsymbol{\epsilon}_y^T\boldsymbol{\epsilon}_y + \boldsymbol{\epsilon}_\theta^T\boldsymbol{\epsilon}_\theta\right). \tag{38}$$

The time derivative of (35) along the solutions of the extended error dynamics (26)-(32) is given by

$$\dot{V}(\boldsymbol{\vartheta}) = \dot{V}_{sys}(\boldsymbol{\vartheta}) + \dot{V}_{cou}(\boldsymbol{\vartheta}) + \dot{V}_{syn}(\boldsymbol{\vartheta}), \tag{39}$$

with

$$\begin{aligned}\dot{V}_{sys}(\boldsymbol{\vartheta}) &= -k_x\mathbf{e}_x^T\mathbf{e}_x - \mathbf{e}_x^T\mathbf{C}\boldsymbol{\zeta}_x - k_\theta\mathbf{e}_\theta^T\mathbf{e}_\theta \\ &\quad - \boldsymbol{\gamma}_{\sin\theta}^T\mathbf{B}\mathbf{e}_y, \end{aligned}\tag{40}$$

$$\dot{V}_{cou}(\boldsymbol{\vartheta}) = -\alpha\boldsymbol{\zeta}_x^T\boldsymbol{\zeta}_x + \mu\boldsymbol{\zeta}_x^T\hat{\mathbf{L}}\boldsymbol{\epsilon}_x, \tag{41}$$

$$\begin{aligned}\dot{V}_{syn}(\vartheta) &= -k_x\boldsymbol{\epsilon}_x^T\boldsymbol{\epsilon}_x - \boldsymbol{\epsilon}_x^T\mathbf{D}\mathbf{C}\boldsymbol{\zeta}_x - k_\theta\boldsymbol{\epsilon}_\theta^T\boldsymbol{\epsilon}_\theta \\ &\quad + \boldsymbol{\epsilon}_y^T\mathbf{D}\boldsymbol{\gamma}_{\sin\theta} + W, \end{aligned}\tag{42}$$

where

$$\begin{aligned}W &= \boldsymbol{\epsilon}_x^T\mathbf{D}\left(\Omega_r\mathbf{e}_y + k_\theta\mathbf{e}_{y\theta} + \Gamma_{\mathrm{sinc}\,\theta}\Gamma_\alpha\mathbf{e}_{y^2}\right) \\ &\quad - \boldsymbol{\epsilon}_y^T\mathbf{D}\left(\Omega_r\mathbf{e}_x + k_\theta\mathbf{e}_{x\theta} + \Gamma_{\mathrm{sinc}\,\theta}\Gamma_\alpha\mathbf{e}_{xy}\right) \\ &\quad - \boldsymbol{\epsilon}_\theta^T\mathbf{D}\Gamma_{\mathrm{sinc}\,\theta}\Gamma_\alpha\mathbf{e}_y, \end{aligned}\tag{43}$$

$\mathbf{B} = \mathrm{diag}\left(Kk_{y_1}/\alpha_1 - 1, \ldots, Kk_{y_N}/\alpha_N - 1\right)$.

Also, it is considered that $\Gamma_{\mathrm{sinc}\,\theta}\mathbf{e}_\theta = \boldsymbol{\gamma}_{\sin\theta}$ and $\mathbf{e}_y^T\boldsymbol{\gamma}_{\sin\theta} = \boldsymbol{\gamma}_{\sin\theta}^T\mathbf{e}_y$ to simplify (40). Finally, a compact form of (39) is obtained after replacing (40)-(42), this is

$$\begin{aligned}\dot{V}(\boldsymbol{\vartheta}) = -\boldsymbol{\xi}_x^T\mathbf{H}\boldsymbol{\xi}_x - k_\theta\boldsymbol{\xi}_\theta^T\boldsymbol{\xi}_\theta - \left(\mathbf{e}_y^T\mathbf{B} - \boldsymbol{\epsilon}_y^T\mathbf{D}\right)\boldsymbol{\gamma}_{\sin\theta} \\ -\boldsymbol{\epsilon}^T\mathbf{M}\mathbf{e}_{xy\theta}, \end{aligned}\tag{44}$$

where $\boldsymbol{\xi}_x = [\mathbf{e}_x^T, \boldsymbol{\epsilon}_x^T, \boldsymbol{\zeta}_x^T]^T$, $\boldsymbol{\xi}_\theta = [\mathbf{e}_\theta^T, \boldsymbol{\epsilon}_\theta^T]^T$, $\boldsymbol{\epsilon} = [\boldsymbol{\epsilon}_x^T,\ \boldsymbol{\epsilon}_y^T,\ \boldsymbol{\epsilon}_\theta^T]^T$, $\mathbf{e}_{xy\theta} = [\mathbf{e}_x^T,\ \mathbf{e}_{xy}^T,\ \mathbf{e}_{x\theta}^T,\ \mathbf{e}_y^T,\ \mathbf{e}_{y^2}^T,\ \mathbf{e}_{y\theta}^T]^T$ and

$$\mathbf{H} = \begin{bmatrix} k_x\mathbf{I}^{N\times N} & \mathbf{0}^{N\times\vartheta} & \mathbf{C} \\ \mathbf{0}^{\vartheta\times N} & k_x\mathbf{I}^{\vartheta\times\vartheta} & \mathbf{D}\mathbf{C} \\ \mathbf{0}^{N\times N} & -\mu\hat{\mathbf{L}} & \alpha\mathbf{I}^{N\times N} \end{bmatrix}, \tag{45}$$

$$\mathbf{M} = \begin{bmatrix} \mathbf{0}^{\vartheta\times 3N} & -\mathbf{M}_{12} \\ \mathbf{M}_{12} & \mathbf{0}^{\vartheta\times 3N} \\ \mathbf{0}^{\mathrm{card}(\vartheta\times 3N} & \mathbf{M}_{32} \end{bmatrix}, \tag{46}$$

with $\vartheta = \mathrm{card}(\mathcal{N})$, $\mathbf{0} \in \mathbb{R}^{n\times m}$ is a null matrix, and $\mathbf{M}_{12} = [\mathbf{D}\Omega_r\ \ \mathbf{D}\Gamma_{\mathrm{sinc}\,\theta}\Gamma_\alpha\ \ k_\theta\mathbf{D}]$ and $\mathbf{M}_{32} = [\mathbf{D}\Gamma_{\mathrm{sinc}\,\theta}\Gamma_\alpha\ \ \mathbf{0}^{\vartheta\times 2N}]$. Moreover, $\mathbf{H}$ is a positive definite matrix for $\mu > 0$.

In (44) it is considered the following facts:

- The term $\left(\mathbf{e}_y^T\mathbf{B} - \boldsymbol{\epsilon}_y^T\mathbf{D}\right)\boldsymbol{\gamma}_{\sin\theta}$ is bounded because the elements in $\mathbf{B}$ have an operating range which depends on the controller gain k_y, i.e. $b_{ii} \in (-1, k_y - 1]$, $i = 1, \ldots, N$, and $\mathbf{D}$ has only zeros and ones. On the other hand, the elements in $\boldsymbol{\gamma}_{\sin\theta}$ are bounded by $\boldsymbol{\gamma}_{\sin\theta_i} \in [-v_{r_i},\ v_{r_i}]$, $i = 1, \ldots, N$.
- Matrix $\mathbf{M}$ is also bounded. The terms $\mathbf{D}\Omega_r$ and $k_\theta\mathbf{D}$ in $\mathbf{M}_{12}$ are bounded by the reference angular-velocities and gain k_θ, respectively. Also, the terms in $\Gamma_{\mathrm{sinc}\,\theta}$ and Γ_α are bounded because $\mathrm{sinc}\,e_{\theta_i} \in (0, 1]$ and $Kky/\alpha_i \in (0, k_y]$, $i = 1, \ldots, N$.
- Moreover, these terms tend to zero when the trajectories are reached. Therefore, (44) is semidefinite negative along ξ_x and ξ_θ trajectories as

$$\dot{V} \leq -\boldsymbol{\xi}_x^T\mathbf{H}\boldsymbol{\xi}_x - k_\theta\boldsymbol{\xi}_\theta^T\boldsymbol{\xi}_\theta. \tag{47}$$

Now, the Lemma of Barbalat is used to prove that the close-loop system (26)-(32) converges globally asymptotically to zero. The following bounds are found after integrating (47)

$$0 \geq \int_0^\infty dV(\boldsymbol{\vartheta}(t)) = -\int_0^\infty \left[\boldsymbol{\xi}_x^T\mathbf{H}\boldsymbol{\xi}_x + k_\theta\boldsymbol{\xi}_\theta^T\boldsymbol{\xi}_\theta\right]\mathrm{d}t, \tag{48}$$

where $V(\boldsymbol{\vartheta}(t))$ is lower bounded by the initial conditions $(\boldsymbol{\vartheta}(0) = [\mathbf{e}_x^T(0),\ \mathbf{e}_y^T(0),\ \mathbf{e}_\theta^T(0),\ \boldsymbol{\zeta}_x^T(0),\ \boldsymbol{\epsilon}_x^T(0),\ \boldsymbol{\epsilon}_y^T(0),\ \boldsymbol{\epsilon}_\theta^T(0)]^T)$, i.e. it exists and it is finite. Then,

$$\lim_{t\to\infty}\left[\boldsymbol{\xi}_x^T\mathbf{H}\boldsymbol{\xi}_x + k_\theta\boldsymbol{\xi}_\theta^T\boldsymbol{\xi}_\theta\right] = 0, \tag{49}$$

which implies

$$\lim_{t\to\infty}\left[\|\boldsymbol{\xi}_x\|_1 + \|\boldsymbol{\xi}_\theta\|_1\right] = 0. \tag{50}$$

The above equation implies that

$$\lim_{t\to\infty}(\mathbf{e}_x, \mathbf{e}_\theta, \boldsymbol{\epsilon}_x, \boldsymbol{\epsilon}_\theta, \boldsymbol{\zeta}_x) = (\mathbf{0}, \mathbf{0}, \mathbf{0}, \mathbf{0}, \mathbf{0}). \tag{51}$$

The next step is to show that the remaining errors also vanish asymptotically. For this, it is enough to show that $\mathbf{e}_y = 0$. To show this, let replace (51) into the set of equations (26), which yields

$$\dot{\mathbf{e}}_x = \Omega_r\mathbf{e}_y + \Gamma_{\mathrm{sinc}\,\theta}\Gamma_\alpha\mathbf{e}_{y^2}. \tag{52}$$

Furthermore, note that (51) also implies that $\dot{\mathbf{e}}_x = 0$. Therefore, the only solution of (52) satisfying this is

$$\mathbf{e}_y = 0. \tag{53}$$

Finally, since $\boldsymbol{\epsilon}_y = \mathbf{D}\mathbf{e}_y$, see (33), it follows that

$$\boldsymbol{\epsilon}_y = 0. \tag{54}$$

Using this and (51), it is clear to see that the only asymptotic solution of system (26)-(32) is

$$(\mathbf{e}_x, \mathbf{e}_y, \mathbf{e}_\theta, \boldsymbol{\zeta}_x, \boldsymbol{\epsilon}_x, \boldsymbol{\epsilon}_y, \boldsymbol{\epsilon}_\theta) = (\mathbf{0}, \mathbf{0}, \mathbf{0}, \mathbf{0}, \mathbf{0}, \mathbf{0}, \mathbf{0}). \tag{55}$$

□

TABLE 1. Values of the controller gains.

Parameter	Value
k_x	$1.7\ s^{-1}$
k_y	$30\ m^{-2}$
k_θ	$1\ s^{-1}$
K	$1\ m$

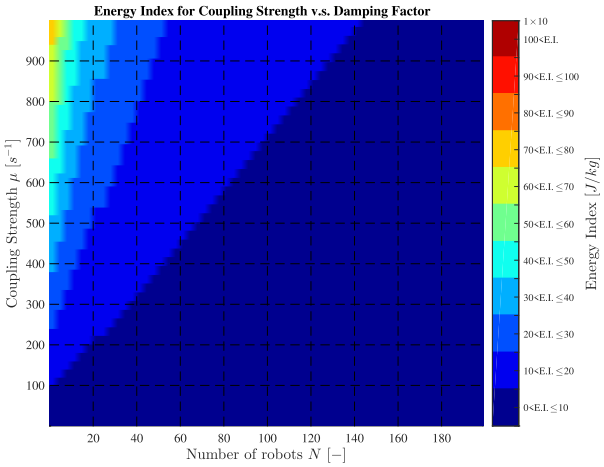

FIGURE 3. Energy index of system (1) with controls (20)-(24), as a function of μ and α.

IV. PERFORMANCE OF THE PROPOSED SCHEME IN TERMS OF AN ENERGY-LIKE INDEX

In this section, the performance of the proposed controller (20)-(24) is investigated by means of numerical simulations, as a function of the following energy-like index $E.I.$ [47]

$$E.I. = \frac{1}{2}\int_0^T \sum_{i=1}^{N}(v_i^2 + R^2\omega_i^2)\mathrm{d}t \tag{56}$$

where R is the radius of the transmission axis, and v_i, ω_i $(i = 1, \ldots, N)$ are the linear and angular velocities, respectively.

The study is conducted for an all-to-all network topology, and is divided in two cases:

a) impact of dynamic coupling parameters
b) performance as a function of the number of robots in the network.

In all the cases the VC trajectory is a parameterized circle, i.e.

$$\mathbf{p}_{vc}(t) = r_{vc}\begin{bmatrix}\cos(\theta_{vc}(t))\\ \sin(\theta_{vc}(t))\end{bmatrix},\ \theta_{vc}(t) = \omega_{vc}t, \tag{57}$$

where $r_{vc} = 1.4$ m is the distance between the origin of GRF and the VC, and $\omega_{vc} = 2\pi/\hat{T}$ with $\hat{T} = 100$ s, is the period of the trajectory.

The position of each robot with respect to the VC is described by

$$\hat{\mathbf{p}}_i = \hat{r}_i\begin{bmatrix}\cos\hat{\theta}_i\\ -\sin\hat{\theta}_i\end{bmatrix},\ i = 1, \ldots, N, \tag{58}$$

where $\hat{r}_i = 0.5$ m is the distance between the robot and the VC, and $\hat{\theta}_i = [2(i-1)\pi]/N$ $(i = 1, \ldots, N)$.

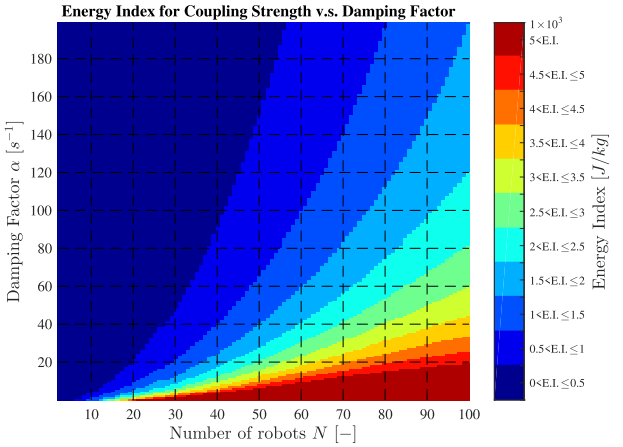

(a) Damping factor α v.s. Number of robots N

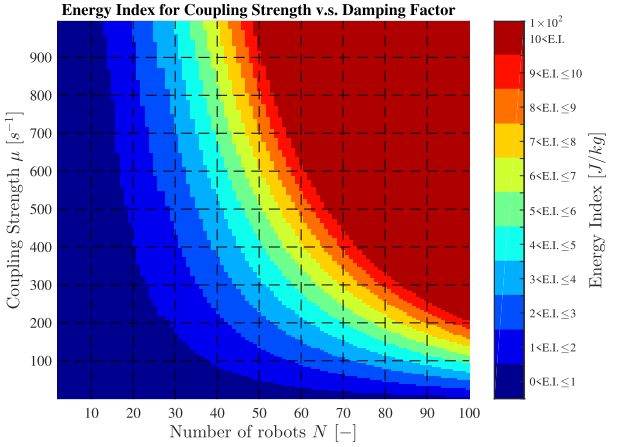

(b) Coupling strength μ v.s. Number of robots N

FIGURE 4. Numerical results for system (1) with controls (20)-(24) as a function of the number of robots N and the parameters α and μ of the dynamic coupling (24). (a) α v.s. N, and (b) μ v.s. N. When the number of robots is large and μ is fixed, the energy index can be lowered by increasing α (top figure). In contrast, for a large number of robots and α fixed, reducing the parameter μ results in reducing the energy index.

The initial conditions are computed by

$$\mathbf{q}_i(0) = \begin{bmatrix}\mathbf{p}_{vc}(0) + \mathbf{R}(\theta_{vc}(0))\tilde{\mathbf{p}}_i\\ \arctan\frac{1-\omega_{vc}\hat{p}_{x_i}}{\omega_{vc}\hat{p}_{y_i}}\end{bmatrix}, \tag{59}$$

where $\mathbf{p}_{vc}(t)$, $\theta_{vc}(t)$ and $\omega_{vc}(t)$ are defined in (57) and $\tilde{\mathbf{p}}_i$ is defined by

$$\tilde{\mathbf{p}}_i = \tilde{r}_i\begin{bmatrix}\cos\hat{\theta}_i\\ -\sin\hat{\theta}_i\end{bmatrix},\ i = 1, \ldots, N, \tag{60}$$

with $\tilde{r}_i$ given by

$$\tilde{r}_i = \begin{cases}1\text{ m} & \forall\, i \in \mathcal{S}_{odd},\\ 0.1\text{ m} & \forall\, i \in \mathcal{S}_{even},\end{cases} \tag{61}$$

where $\mathcal{S}_{odd} = \{i \in \mathcal{S} | i = 1, 3, \ldots, N-1\}$ is the odd subset of robots and $\mathcal{S}_{even} = \{i \in \mathcal{S} | i = 2, 4, \ldots, N\}$ is the even subset of robots.

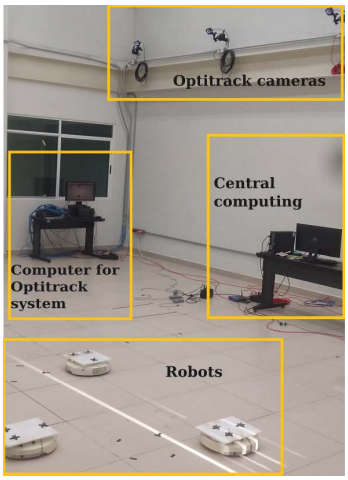

(a) Physical setup

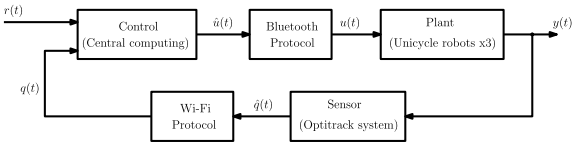

(b) Block diagram of the setup

FIGURE 5. **Experimental setup. The setup is composed by 12 Optitrack cameras, a central computing, and three unicycle robots from the iRobot company. For a reference $r(t)$, the control laws $\hat{u}(t)$ are calculated by the central computer and are sent, via Bluetooth protocol ($u(t)$), to the robots whose output is a pose ($y(t)$). The sensor (Optitrack system) obtains the real pose of the robots $\hat{q}(t)$ which is sent to the central computing via Wi-Fi protocol ($q(t)$).**

The gains of the controller (20)-(24) are summarized in Table 1. The reference orientation θ_{r_i}, is obtained by integrating the angular velocity ω_{r_i} in (9). Finally, the whole system is integrated by using the Runge-Kutta method with $T = 100$ s and a time-step $\Delta t = 2$ ms.

A. IMPACT OF DYNAMIC COUPLING PARAMETERS

The study presented here considers 4 robots, i.e. $N = 4$. Furthermore, the initial conditions are given by (59) and the parameters α and μ in the dynamic coupling (24) are varied as follows

$$0.01 \leq \alpha \leq 200, \ \Delta\alpha = 1 \text{ s}^{-1}, \tag{62}$$

$$0.01 \leq \mu \leq 1000, \ \Delta\mu = 20 \text{ s}^{-1}. \tag{63}$$

The results are shown in Fig. 3. It can be seen that there exist an inverse relationship between the coupling parameters: for small α and large μ, the energy index is large, whereas for large α and small μ, the energy index is low. Thus, in order to have a minimum energy index in the controller, the gains α and μ in (24) should be chosen within the navy blue region in Fig. 3.

B. PERFORMANCE AS A FUNCTION OF THE NUMBER OF ROBOTS IN THE NETWORK

Now, the influence of the number of robots in the energy index of the controller is investigated. To this end, the number

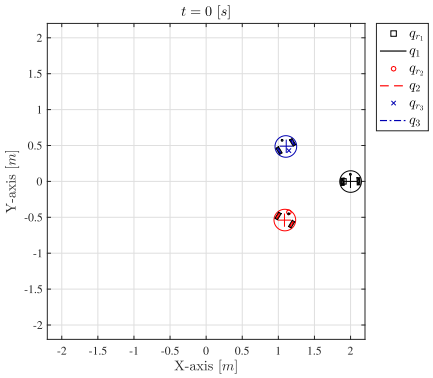

(a) $t = 0$ s

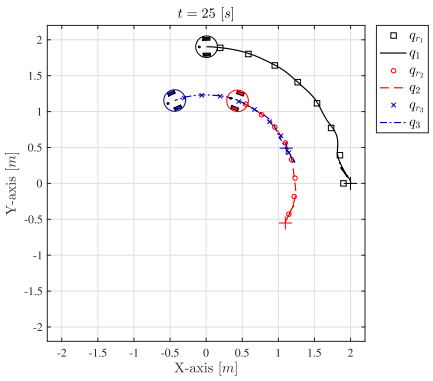

(b) $t = 25$ s

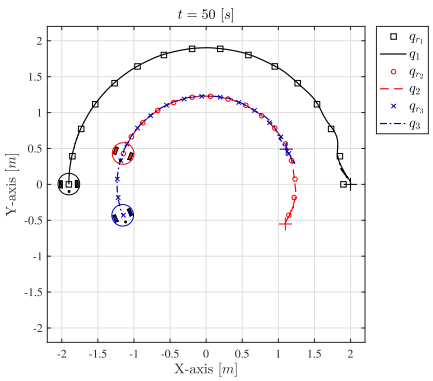

(c) $t = 50$ s

FIGURE 6. **XY-plane for the experimental results. The □, ∘ and × markers are the reference trajectories for the first, second and third robots, respectively. Also, the –, – – and –· lines are for the real positions of first, second and third robots, respectively, the initial conditions are marked with +.**

of robots is varied as follows

$$2 \leq N \leq 100, \ \Delta N = 2, \tag{64}$$

In a first study, all parameters are as before, except for α, which is varied in the interval $0.01 \leq \alpha \leq 200$ in intervals of $\Delta\alpha = 1 \text{ s}^{-1}$ and μ is set to $\mu = 1000 \text{ s}^{-1}$, whereas in the second study, α is fixed to $\alpha = 60 \text{ s}^{-1}$ and μ is varied in the interval $0.01 \leq \mu \leq 1000$ in steps of $\Delta\mu = 5 \text{ s}^{-1}$. Finally,

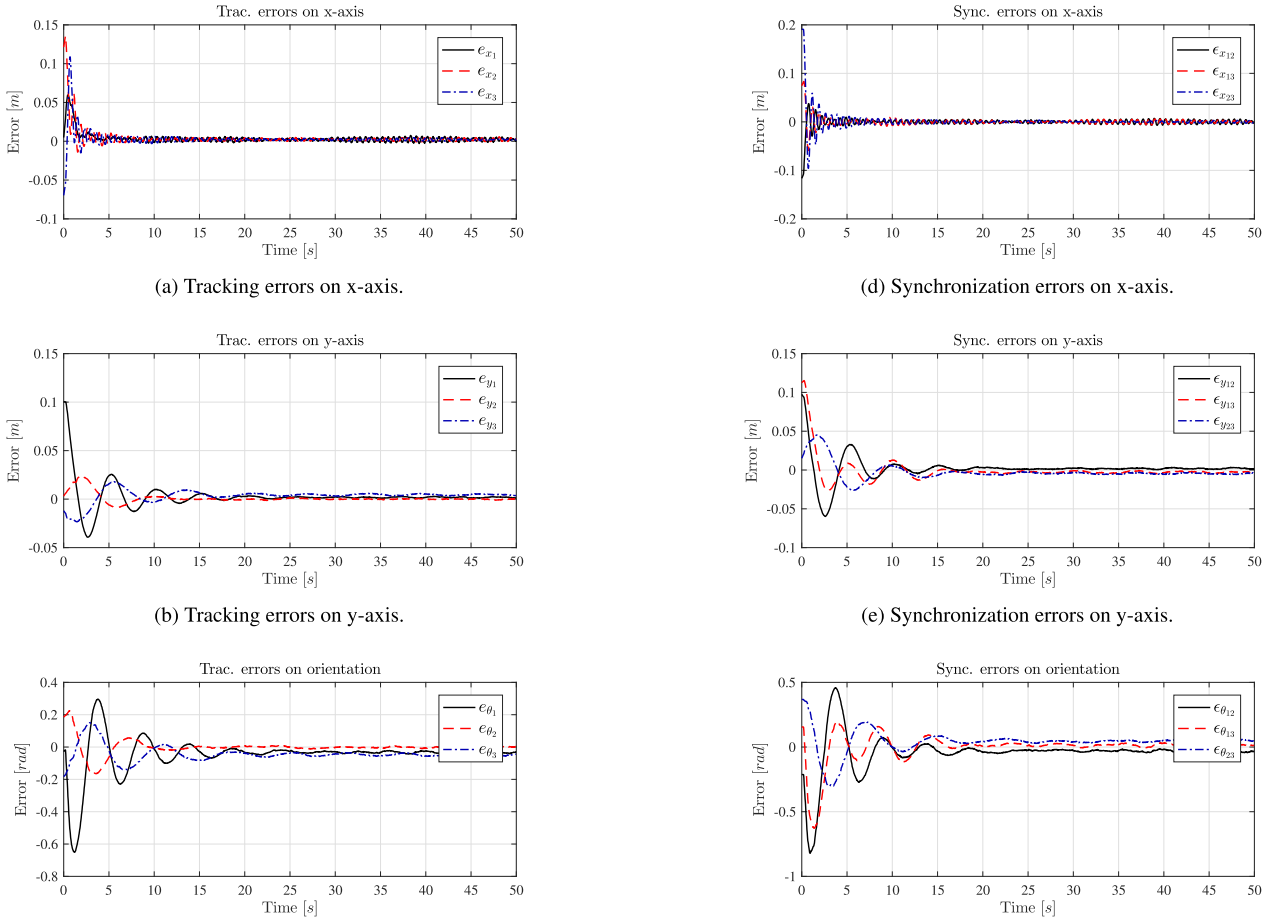

(a) Tracking errors on x-axis.

(b) Tracking errors on y-axis.

(c) Tracking errors on orientation.

(d) Synchronization errors on x-axis.

(e) Synchronization errors on y-axis.

(f) Synchronization errors on orientation.

FIGURE 7. Experimental results. (a)-(c) show the tracking errors for the x-axis, y-axis and orientation, respectively, and (d)-(f) show the corresponding synchronization errors. The tracking errors show the individual behaviour of the robots and the synchronization errors show the collective behaviour.

similar to the previous case, the initial conditions are given in (59).

The obtained results are shown in Fig. 4a and Fig. 4b, respectively, from which two opposite effects can be seen:

- **a)** For lowering the energy index when the number of robots is large and μ is fixed, it seems necessary to **increase** the damping factor α, see Fig. 4a.
- **b)** In contrast, when the number of robots is large and α is fixed, lowering the energy index of the controller requires to **decrease** the coupling strength μ.

V. EXPERIMENTAL RESULTS

This section provides an experimental validation for the proposed controller (20)-(24) for a group of $N = 3$ robots in an all-to-all configuration.

The experimental setup, which is depicted in Fig. 5, is composed by an Optitrack system with 12 cameras to get the pose of each robot and a central computer to calculate its control law, see Fig. 5a. The Optitrack system and the central computer are connected by the Ethernet protocol, whereas the central computer uses the Bluetooth protocol to send the control law to each robot, see Fig. 5b. The robots are the iRobot model 4812 whose axis have a length of $b_w = 0.2605$ m and a limit velocity of ± 0.5 rad/s. The controller gains are in Table 1 and the coupling parameters are $\alpha = 30\ \text{s}^{-1}$ and $\mu = 75\ \text{s}^{-1}$. The VC trajectory is a circle, see (57), with $\hat{\mathbf{p}}_i$ $(i = 1, 2, 3)$ defined in (58) for $N = 3$. The reference orientation is computed by integrating the angular velocity (ω_{r_i}) given in (9). The experiment time is $T = 50$ s with a sample frequency $F_s = 30$ Hz.

Fig. 6 shows snapshots of the trajectories of the robots in the XY-plane, for an experiment lasting 50 s. The robots reach their respective trajectories after some transient and they keep the formation along the experiment.

Figs. 7a-7c show the tracking errors, whereas the synchronization errors are presented in Figs. 7d-7f. It can be seen that within the first 10 s of the experiment all the errors almost vanish. Particularly, the errors on the x-axis (Figs. 7a and 7d) converge faster than the errors on the y-axis (Figs. 7b and 7e) and orientation (Figs. 7c and 7d), this is attributed to the fact that the coupling is only applied in the x-axis direction.

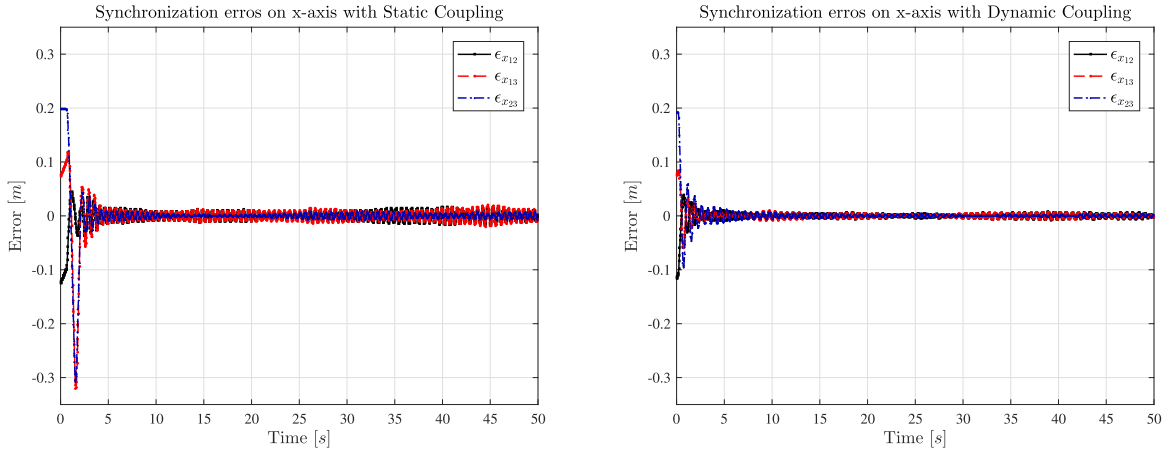

(a) Synchronization errors on the x-axis with Static coupling.

(b) Synchronization errors on the y-axis with Dynamic coupling.

FIGURE 8. Comparison of synchronization errors on the x-axis. After transient, the synchronization errors are relatively smaller for the proposed dynamic controller (20)**-24 than those corresponding to the static controller** (65)-(66)**.**

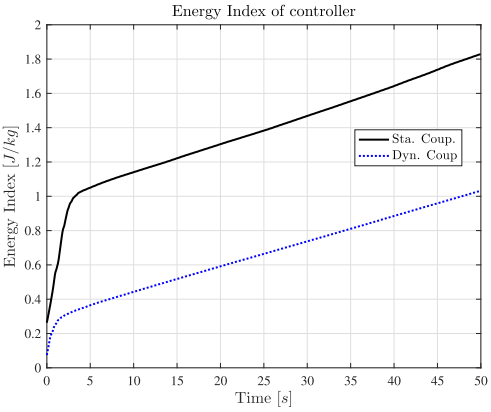

FIGURE 9. Energy index for the traditional static controller (65)-(66) **(solid black line) and the proposed dynamic controller** (20)-(24) **(blue dotted line).**

VI. COMPARISON TO A STATIC CONTROLLER

In this section, the performance of the proposed controller (20)-(24) is compared against the following static controller reported in [10]

$$v_i = v_{r_i}\cos e_{\theta_i} + k_x e_{x_i} + C_x \sum_{(i,j)\in\mathcal{N}} l_{ij}\epsilon_{x_{ij}}, \tag{65}$$

$$\omega_i = \omega_{r_i} + k_\theta e_{\theta_i} + \frac{Kk_y v_{r_i}}{\beta_i} e_{y_i}\,\mathrm{sinc}\, e_{\theta_i}, \tag{66}$$

where v_{r_i} and ω_{r_i} are the reference velocities defined in (9); k_x, k_y and k_θ are gains for the nonlinear tracking control; C_x is the coupling strength for the static coupling on the x-axis and l_{ij} are elements of the Laplacian matrix (15), and $\epsilon_{x_{ij}}$ is the synchronization error on the x-axis defined in (17). $K \in \mathbb{R}_+$ is a constant and β_i is

$$\beta_i = \sqrt{K^2 + e_{x_i}^2 + e_{y_i}^2 + \sum_{(i,j)\in\mathcal{N}} \epsilon_{x_{ij}}^2}. \tag{67}$$

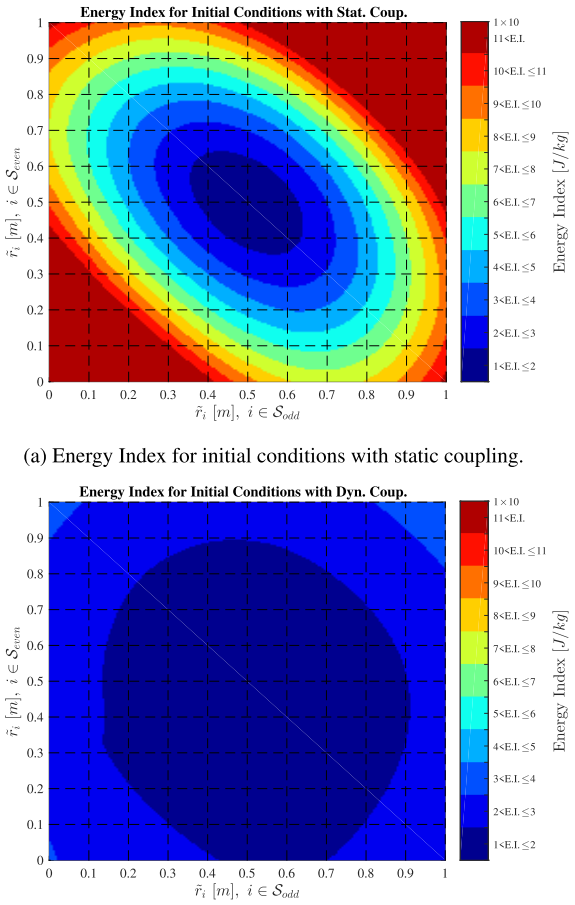

(a) Energy Index for initial conditions with static coupling.

(b) Energy Index for initial conditions with dynamic coupling.

FIGURE 10. Performance of the controllers for large initial conditions in terms of the energy index (56)**. a) Controller with static coupling** (65)-(66) **reported in [10]. b) Proposed controller** (20)-(21) **with dynamic coupling** (24)**.**

Note that the static controller (65)-(66) uses tracking and synchronization errors in the term β_i, see (67). In contrast, the

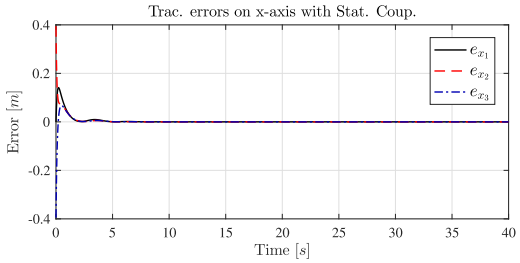

(a) Tracking errors on x-axis with static coupling.

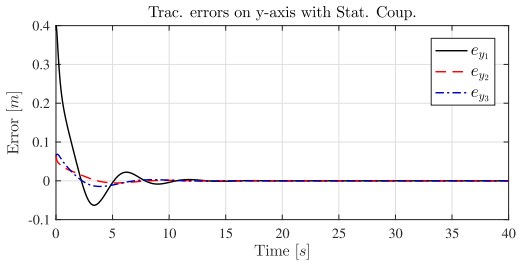

(b) Tracking errors on y-axis with static coupling.

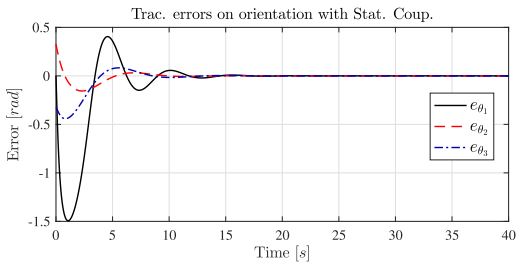

(c) Tracking errors on orientation with static coupling.

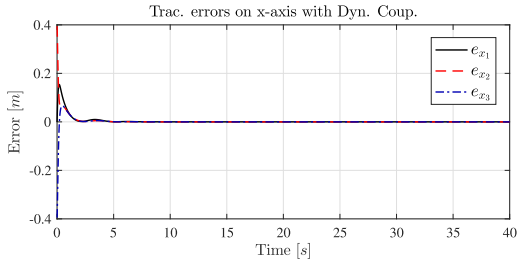

(d) Tracking errors on x-axis with dynamic coupling.

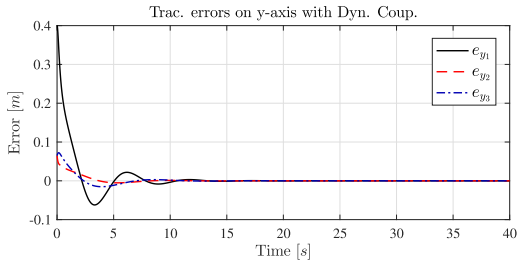

(e) Tracking errors on y-axis with dynamic coupling.

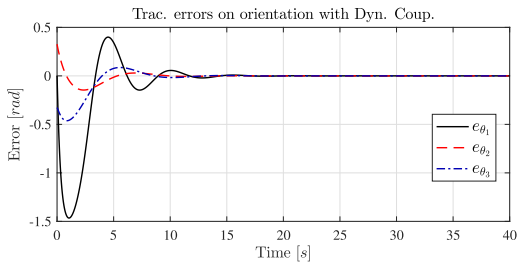

(f) Tracking errors on orientation with dynamic coupling.

FIGURE 11. Numerical results for a large initial conditions. (a)-(c) show the tracking errors for the x-axis, y-axis and orientation, respectively, with the static controller (65)-(66) and (d)-(f) show the corresponding tracking errors for the dynamic controller (65)-(24). Both controllers have a similar performance. The difference, however, is in the energy required by the controllers to achieve the desired behavior, as already shown in Fig. 10.

dynamic controller (20)-(24) only uses the tracking errors in α_i, see (22).

A. EXPERIMENTAL COMPARISON

For the sake of comparison, the same experiment presented in the previous section has been conducted, but this time using the static control (65)-(66), and using the same parameters and initial conditions. The obtained results are presented in Fig. 8a. It can be seen that, after the transient, the synchronization errors are slightly larger than those obtained with the proposed dynamic controller, which are depicted in Figs. 7d, and 8b.

However, the real difference between both controllers can be appreciated when using the proposed energy index (56), as clearly seen in Fig. 9, where the energy index of the proposed dynamic controller (20)-(24), see blue dotted line, is lower than the energy index corresponding to the traditional static controller (65)-(66), see solid black line.

Finally, it is worth mentioning that during the experiments, it was found that the static controller (65)-(66) saturates faster the robots, when increasing the coupling strength, than the proposed controller (20)-(24).

B. LARGE INITIAL CONDITIONS

In this section, the performance of the proposed controller (20)-(21) with dynamic coupling (24) is numerically compared against the static controller (65)-(66), for large initial conditions. The comparison is made in terms of the energy index (56).

The controller gains are given in Table 1, the coupling parameters are those used for experiments: $C_x = 3\ \mathrm{s}^{-1}$ for the static coupling in (65)-(66), and $\alpha = 30\ \mathrm{s}^{-1}$ and $\mu = 75\ \mathrm{s}^{-1}$ for the dynamic coupling (24). Finally, the initial conditions are established by using (59) with

$$0 \leq r_i \leq 1\ \Delta r_i = 0.005\ m\ \forall\ i \in \mathcal{S}_{odd}, \tag{68}$$

$$0 \leq r_i \leq 1\ \Delta r_i = 0.005\ m\ \forall\ i \in \mathcal{S}_{even}, \tag{69}$$

The obtained results are shown in Fig. 10. It can be seen that for the case of the static controller (65)-(66), the energy index increases considerably as the initial conditions are fare

away from the desired trajectory. In contrast, for the proposed controller with dynamic coupling (24), the value of the energy index is almost independent of the initial conditions and remains small.

Hence, with respect to the energy index (56), the dynamic controller presented here requires less energy to achieve the coordination task than the static controller (65)-(66). Finally, note that numerical results shown in Fig. 10b are in good agreement with the experimental results shown in Fig. 9: in both cases the energy index of the proposed controller is smaller.

On the other hand, the results in terms of tracking errors show the behaviour is equal with both couplings for the large initial conditions $r_i = 0.9$, $(i = 1, 2, 3)$, see Fig. 11. The tracking errors on the x-axis reach to zero in lower time, see Figs. 11a for static coupling and 11b for dynamic coupling, whereas the tracking errors on the y-axis and orientation take long time to reach the origin, see Figs. 11b and 11c, respectively for the static coupling and Figs. 11e and Figs. 11f, respectively, for the dynamic one.

VII. DISCUSSIONS AND CONCLUSION

This work has presented a coordination scheme for unicycle robots using dynamic couplings. The proposed strategy (20)-(24), is composed by two parts: a nonlinear controller for tracking and a dynamic coupling for synchronization/coordination.

The stability analysis shows that the extended error dynamics, which are composed by the tracking and synchronization errors, are globally asymptotically stable, independently on the number of robots.

The obtained numerical and experimental results show the following: for the proposed coordination scheme, the synchronization errors in steady state are lower than the ones observed when using traditional coordination scheme with static coupling given in (65)-(66), see Fig. 8. Moreover, the energy index of the proposed dynamic coupling is lower than the index obtained with a static coupling regardless of the initial conditions of the robots, see Figs. 9 and 10.

In summary, the results presented here have shown that the proposed coordination strategy exhibits a good performance and it can be seen as a potential alternative for coordinating multi-agent systems. It would be interesting to formally investigate the applicability of this coordination scheme in the context of other MAS. This, however, is the topic of other ongoing research.

REFERENCES

[1] J. P. Ramirez, L. A. Olvera, H. Nijmeijer, and J. Alvarez, "The sympathy of two pendulum clocks: Beyond Huygens observations," *Sci. Rep.*, vol. 6, no. 1, p. 23580, Jul. 2016.

[2] Z. Miao, Y.-H. Liu, Y. Wang, G. Yi, and R. Fierro, "Distributed estimation and control for leader-following formations of nonholonomic mobile robots," *IEEE Trans. Autom. Sci. Eng.*, vol. 15, no. 4, pp. 1946–1954, Oct. 2018.

[3] A. Pikovsky, M. Rosenblum, and J. Kurths, *Synchronization. An Universal Concept in Nonlinear Sciences*. Cambridge, U.K.: Cambridge Univ. Press, 2001, pp. 1–172.

[4] A. A. A. Rasheed, M. N. Abdullah, and A. S. Al-Araji, "A review of multi-agent mobile robot systems applications," *Int. J. Elec. Comp. Eng. (IJECE)*, vol. 12, no. 4, pp. 3517–3529, 2022.

[5] H. Eberle, S. J. Nasuto, and Y. Hayashi, "Synchronization-based control for a collaborative robot," *Roy. Soc. Open Sci.*, vol. 7, no. 12, Dec. 2020, Art. no. 201267.

[6] J. Obregón and A. Morales, "Synchronized mobile manipulators for kinematic cooperative tasks: Control design and analysis," *IFAC-PapersOnLine*, vol. 53, no. 2, pp. 9074–9079, 2020.

[7] S. C. Spry, A. R. Girard, and J. K. Hedrick, "Convoy protection using multiple unmanned aerial vehicles: Organization and coordination," in *Proc. Amer. Control Conf.*, Jun. 2005, pp. 3524–3529.

[8] H. Gutiérrez, A. Morales, and H. Nijmeijer, "Synchronization control for a swarm of unicycle robots: Analysis of different controller topologies," *Asian J. Control*, vol. 19, no. 5, pp. 1822–1833, 2017.

[9] D. Kostic, S. Adinandra, J. Caarls, N. van de Wouw, and H. Nijmeijer, "Saturated control of time-varying formations and trajectory tracking for unicycle multi-agent systems," in *Proc. 49th IEEE Conf. Decis. Control (CDC)*, Dec. 2010, pp. 4054–4059.

[10] A. Morales and H. Nijmeijer, "Merging strategy for vehicles by applying cooperative tracking control," *IEEE Trans. Intell. Transp. Syst.*, vol. 17, no. 12, pp. 3423–3433, Dec. 2016.

[11] J. Qin, S. Wang, Y. Kang, and Q. Liu, "Circular formation algorithms for multiple nonholonomic mobile robots: An optimization-based approach," *IEEE Trans. Ind. Electron.*, vol. 66, no. 5, pp. 3693–3701, May 2019.

[12] R. A. García, L. Orihuela, P. Millán, F. R. Rubio, and M. G. Ortega, "Guaranteed estimation and distributed control of vehicle formations," *Int. J. Control*, vol. 93, no. 11, pp. 2729–2742, Nov. 2020.

[13] N. T. Hung, F. F. C. Rego, and A. M. Pascoal, "Cooperative distributed estimation and control of multiple autonomous vehicles for range-based underwater target localization and pursuit," *IEEE Trans. Control Syst. Technol.*, vol. 30, no. 4, pp. 1433–1447, Jul. 2022.

[14] A. Jenabzadeh and B. Safarinejadian, "Distributed estimation and control for nonlinear multi-agent systems in the presence of input delay or external disturbances," *ISA Trans.*, vol. 98, pp. 198–206, Mar. 2020.

[15] M. A. Lewis and K.-H. Tan, "High precision formation control of mobile robots using virtual structures," *Auto. Robots*, vol. 4, no. 4, pp. 387–403, 1997.

[16] A. Sadowska, T. van den Broek, H. Huijberts, N. van de Wouw, D. Kostić, and H. Nijmeijer, "A virtual structure approach to formation control of unicycle mobile robots using mutual coupling," *Int. J. Control*, vol. 84, no. 11, pp. 1886–1902, 2011.

[17] X. Chu, Z. Peng, G. Wen, and A. Rahmani, "Distributed formation tracking of multi-robot systems with nonholonomic constraint via event-triggered approach," *Neurocomputing*, vol. 275, pp. 121–131, Jan. 2018.

[18] X. Chen, F. Huang, Y. Zhang, Z. Chen, S. Liu, Y. Nie, J. Tang, and S. Zhu, "A novel virtual-structure formation control design for mobile robots with obstacle avoidance," *Appl. Sci.*, vol. 10, no. 17, p. 5807, Aug. 2020.

[19] Y. Liu, D. Yao, H. Li, and R. Lu, "Distributed cooperative compound tracking control for a platoon of vehicles with adaptive NN," *IEEE Trans. Cybern.*, vol. 52, no. 7, pp. 7039–7048, Jul. 2022.

[20] D. Qin, A. Liu, D. Zhang, and H. Ni, "Formation control of mobile robot systems incorporating primal-dual neural network and distributed predictive approach," *J. Franklin Inst.*, vol. 357, no. 17, pp. 12454–12472, Nov. 2020.

[21] J. Zelenka, T. Kasanický, M. Bundzel, and R. Andoga, "Self-adaptation of a heterogeneous swarm of mobile robots to a covered area," *Appl. Sci.*, vol. 10, no. 10, p. 3562, May 2020.

[22] D. Yu, C. L. P. Chen, and H. Xu, "Fuzzy swarm control based on sliding-mode strategy with self-organized omnidirectional mobile robots system," *IEEE Trans. Syst., Man, Cybern. Syst.*, vol. 52, no. 4, pp. 2262–2274, Apr. 2022.

[23] J. Hu, P. Bhowmick, and A. Lanzon, "Group coordinated control of networked mobile robots with applications to object transportation," *IEEE Trans. Veh. Technol.*, vol. 70, no. 8, pp. 8269–8274, Aug. 2021.

[24] J. Hu, A. E. Turgut, B. Lennox, and F. Arvin, "Robust formation coordination of robot swarms with nonlinear dynamics and unknown disturbances: Design and experiments," *IEEE Trans. Circuits Syst. II, Exp. Briefs*, vol. 69, no. 1, pp. 114–118, Jan. 2022.

[25] Y. Cao, W. Yu, W. Ren, and G. Chen, "An overview of recent progress in the study of distributed multi-agent coordination," *IEEE Trans. Ind. Informat.*, vol. 9, no. 1, pp. 427–438, Feb. 2012.

[26] L. Liu, J. Yu, J. Ji, Z. Miao, and J. Zhou, "Cooperative adaptive consensus tracking for multiple nonholonomic mobile robots," *Int. J. Syst. Sci.*, vol. 50, no. 8, pp. 1556–1567, Jun. 2019.
[27] P. Lu, H. Wang, F. Zhang, W. Yu, and G. Chen, "Formation control of nonholonomic mobile robots using distributed estimators," *IEEE Trans. Circuits Syst. II, Exp. Briefs*, vol. 67, no. 12, pp. 3162–3166, Dec. 2020.
[28] J. Fu, T. Huang, and G. Wen, "Global leader-following control of multiple non-holonomic mobile robots with input saturation," in *Proc. 15th Int. Conf. Control, Autom., Robot. Vis. (ICARCV)*, Nov. 2018, pp. 862–867.
[29] V. L. S. Freitas, S. Yanchuk, M. Zaks, and E. E. N. Macau, "Synchronization-based symmetric circular formations of mobile agents and the generation of chaotic trajectories," *Commun. Nonlinear Sci. Numer. Simul.*, vol. 94, Mar. 2021, Art. no. 105543.
[30] X. Chu, Z. Peng, G. Wen, and A. Rahmani, "Robust fixed-time consensus tracking with application to formation control of unicycles," *IET Control Theory Appl.*, vol. 12, no. 1, pp. 53–59, 2018.
[31] X. Zhang, Z. Peng, S. Yang, G. Wen, and A. Rahmani, "Distributed fixed-time consensus-based formation tracking for multiple nonholonomic wheeled mobile robots under directed topology," *Int. J. Control*, vol. 94, no. 1, pp. 248–257, Jan. 2021.
[32] J. Dai and G. Guo, "Event-triggered leader-following consensus for multi-agent systems with semi-Markov switching topologies," *Inf. Sci.*, vol. 459, pp. 290–301, Aug. 2018.
[33] X. Liu, K. Zhang, and W.-C. Xie, "Consensus seeking in multi-agent systems via hybrid protocols with impulse delays," *Nonlinear Anal. Hybrid Syst.*, vol. 25, pp. 90–98, Aug. 2017.
[34] X. Liu, K. Zhang, and W.-C. Xie, "Consensus of multi-agent systems via hybrid impulsive protocols with time-delay," *Nonlinear Anal., Hybrid Syst.*, vol. 30, pp. 134–146, Nov. 2018.
[35] H. Shen, Y. Wang, J. Xia, J. H. Park, and Z. Wang, "Fault-tolerant leader-following consensus for multi-agent systems subject to semi-Markov switching topologies: An event-triggered control scheme," *Nonlinear Anal., Hybrid Syst.*, vol. 34, pp. 92–107, Nov. 2019.
[36] X. Li, Y. Tang, and H. R. Karimi, "Consensus of multi-agent systems via fully distributed event-triggered control," *Automatica*, vol. 116, Jun. 2020, Art. no. 108898.
[37] Z. Cheng, D. Yue, S. Hu, H. Ge, and L. Chen, "Distributed event-triggered consensus of multi-agent systems under periodic DoS jamming attacks," *Neurocomputing*, vol. 400, pp. 458–466, Aug. 2020.
[38] A. Barcis and C. Bettstetter, "Beyond sync: Distributed temporal coordination and its implementation in a multi-robot system," in *Proc. IEEE 13th Int. Conf. Self-Adaptive Self-Organizing Syst. (SASO)*, Jun. 2019, pp. 88–96.
[39] A. Barcis and C. Bettstetter, "Sandsbots: Robots that sync and swarm," *IEEE Access*, vol. 8, pp. 218752–218764, 2020.
[40] J. Pena Ramirez, A. Arellano-Delgado, and H. Nijmeijer, "Enhancing master-slave synchronization: The effect of using a dynamic coupling," *Phys. Rev. E, Stat. Phys. Plasmas Fluids Relat. Interdiscip. Top.*, vol. 98, no. 1, Jul. 2018, Art. no. 012208.
[41] N. van de Wouw, E. Lefeber, and I. L. Arteaga, Eds., *Nonlinear Systems. Techniques for Dynamical Analysis and Control*, vol. 470. Cham, Switzerland: Springer, 2017, pp. 81–102.
[42] P. Arena, A. Buscarino, L. Fortuna, and L. Patanè, "Lyapunov approach to synchronization of chaotic systems with vanishing nonlinear perturbations: From static to dynamic couplings," *Phys. Rev. E, Stat. Phys. Plasmas Fluids Relat. Interdiscip. Top.*, vol. 102, no. 1, Jul. 2020, Art. no. 012211.
[43] W. D. Jonge, J. P. Ramirez, and H. Nijmeijer, "Dynamic coupling enhances network synchronization," *IFAC-PapersOnLine*, vol. 52, no. 16, pp. 610–615, 2019.
[44] Z. Li, Z. Duan, G. Chen, and L. Huang, "Consensus of multiagent systems and synchronization of complex networks: A unified viewpoint," *IEEE Trans. Circuits Syst. I, Reg. Papers*, vol. 57, no. 1, pp. 213–224, Jan. 2010.
[45] Z. Li, W. Ren, X. Liu, and M. Fu, "Distributed containment control of multi-agent systems with general linear dynamics in the presence of multiple leaders," *Int. J. Robust Nonlinear Control*, vol. 23, no. 5, pp. 534–547, 2013.
[46] J. A. K. Suykens, P. F. Curran, and L. O. Chua, "Master-slave synchronization using dynamic output feedback," *Int. J. Bifurcation Chaos*, vol. 7, no. 3, pp. 671–679, Mar. 1997.
[47] A. V. Oppenheim, A. S. Willsky, and S. H. Nawab, *Signals & Systems*, 2nd ed. Hoboken, NJ, USA: Pretince-Hall, 1997, pp. 1–73.

I. RUIZ-RAMOS was born in Puebla, in 1988. He received the bachelor's degree in electronics engineering from the Tijuana Institute of Technology (ITT) and the M.S. degree in electronics and telecommunication from Scientific Research and Higher Education, CICESE, Ensenada. Currently, he is pursuing the Ph.D. degree with Robotics and Advanced Manufacturing Program, CINVESTAV, Saltillo.

A. MORALES received the B.Sc. degree in chemical-petroleum engineering from Instituto Politécnico Nacional, México, in 1994, and the M.Sc. and Ph.D. degrees in chemical engineering from Universidad Autónoma Metropolitana, Mexico.

She is a Researcher with CINVESTAV, Saltillo Coahuila, Mexico. She has published several journal articles and some international conference papers. Her research interests include control systems engineering, mobile robotics, cooperative control, and robotics in agriculture. Her areas of expertise include nonlinear control and systems, process control, and robotics.

J. PENA RAMIREZ received the Ph.D. degree in mechanical engineering from Eindhoven University of Technology, The Netherlands, in 2013. He is a dynamicist working at the Center for Scientific Research and Higher Education at Ensenada (CICESE). He conducted a posdoctoral stay at the Institute of Industrial Science in Tokyo, Japan. Currently, he is a Specially Appointed Associate Professor with Tokyo Institute of Technology.